Cuadernos de Investigación Geográfica *Geographical Research Letters*	2023	Nº 49	pp. 39-53	EISSN 1697-9540

Copyright © 2023, The authors. This work is licensed under a Creative Commons Attribution 4.0 International License.

http://doi.org/10.18172/cig.5473

SPATIAL CHARACTERIZATION OF CLIMATIC VARIABLES FOR ARICA-PARINACOTA AND TARAPACÁ, CHILE USING TOPOCLIMATIC ANALYSIS

LUIS MORALES-SALINAS[1*], GIORGIO CASTELLARO[2], NORA FREDERIKSEN[1], LUIS F. ROMÁN[3, 5], JOSÉ NEIRA-ROMÁN[4], GUILLERMO FUENTES-JAQUE[1], CRISTIÁN ESCOBAR[1], FELIPE MORALES[1]

[1]*Laboratorio de Investigación en Ciencias Ambientales (LARES), Facultad de Ciencias Agronómicas, Universidad de Chile. Santa Rosa 11315, La Pintana, Santiago. Casilla 1004, Chile.*

[2]*Departamento de Producción Animal, Facultad de Ciencias Agronómicas, Universidad de Chile (Chile). Santa Rosa 11315, La Pintana, Santiago. Casilla 1004, Chile.*

[3]*Facultad de Ciencias Agronómicas Campus Azapa, Universidad de Tarapacá, Arica, Chile.*

[4]*Facultad de Ciencias Agrarias y Forestales, Universidad Católica del Maule, Casilla 617, Curicó, Chile.*

[5]*Departamento de Recursos Hídricos, Facultad de Ingeniería Agrícola, Universidad Nacional Agraria La Molina, Lima, Perú.*

ABSTRACT. In the present study, models were developed to determine the monthly and annual spatio-temporal variation of temperature, precipitation, and solar radiation based on topoclimatic analysis of Arica-Parinacota and Tarapacá in northern Chile. To construct the equations of the topoclimatic model, the data from meteorological stations and physiographic factors (latitude, longitude, altitude, and distance to bodies of water) obtained from a digital terrain model with a resolution of 90 m were compiled in a database. The equations of the topoclimatic model were generated by a stepwise regression with a backward selection technique. The equations for average monthly temperature, precipitation, and solar radiation were determined by linear combinations. The results were statistically significant with coefficients of determination greater than 90%, in addition to being greater than the existing climate databases for this area.

Caracterización espacial de variables climáticas de Arica-Parinacota y Tarapacá, Chile mediante análisis topoclimático

RESUMEN. En el presente estudio se desarrollaron modelos para determinar la variación espaciotemporal mensual y anual de temperatura, precipitación y radiación solar con base en el análisis topoclimático de Arica-Parinacota y Tarapacá en el norte de Chile. Para construir las ecuaciones del modelo topoclimático, se compilaron en una base de datos la información de estaciones meteorológicas y factores fisiográficos (latitud, longitud, altitud y distancia a cuerpos de agua) obtenidos de un modelo digital del terreno con una resolución de 90 m. Las ecuaciones del modelo topoclimático se generaron mediante una regresión escalonada con una técnica de selección hacia atrás. Las ecuaciones para la temperatura media mensual, la precipitación y la radiación solar se determinaron mediante combinaciones lineales. Los resultados fueron estadísticamente significativos con coeficientes de determinación superiores al 90%, siendo más elevados que las bases de datos climáticas existentes para esta área.

Key words: Atacama Desert, Spatial characterization, Topoclimatic analysis.

Palabras clave: desierto de Atacama, caracterización espacial, análisis topoclimático.

Received: 22 May 2022

Accepted: 2 December 2022

***Corresponding author:** Luis Morales-Salinas, Laboratorio de Investigación en Ciencias Ambientales (LARES), Facultad de Ciencias Agronómicas, Universidad de Chile. Santa Rosa 11315, La Pintana, Santiago. Casilla 1004, Chile. E-mail address: lmorales@renare.uchile.cl

1. Introduction

Properly characterizing a territory based on its climatic characteristics are the basis of correct territorial planning more efficient for natural resources, agriculture, and hydrology. This could be enhanced with the implementation of a combination between geographic information systems (GIS) and models (Grunwald, 2009; Grunwald *et al.*, 2011; Kaye *et al.*, 2012; Burkhard and Maes, 2017).

The computer programming has allowed develop algorithms for predict the spatial distribution of climate variables from data of weather stations (Hijmans *et al.*, 2005; Hunter and Meentemeyer, 2005; Fredericksen, 2010; Harris *et al.*, 2014). The topoclimatic analysis studies the relations between climatic and physiographic variables, which describe a climatic zone or area (Kaminski and Radosz, 2005). However, climate mapping is conditioned by the availability and quality of data from meteorological stations distributed spatially in a zone (Skirvin *et al.*, 2003; Morales *et al.*, 2006), instead non spatially distributed stations or discontinued data require to develop models that spatially represent the distribution climatic variables using GIS and environmental modeling, which helps to solve the problems caused by the lack of information in certain areas (Florinsky, 1998; Daly *et al.*, 2008).

The mapping of the Atacama Desert (Arica-Parinacota, Tarapacá, and Antofagasta) is scarce and imprecise for climatic variables (Hijmans *et al.*, 2005; Luebert and Pliscoff, 2018), both with limited applications and inappropriate to climatic zoning with agronomic purposes. The high variability of some topographic variables and the combination of the marine influence and the Pacific Anticyclone that determine the arid conditions in the coast and inner zones (Garreaud *et al.*, 2003), must be considered in the implementation of GIS analysis and modeling to determine the climate zoning (Hijmans *et al.*, 2005; Luebert and Pliscoff, 2018).

The correct climatic characterization of the Atacama Desert needs complementary information, as worldwide databases. Different databases in the literature could be used such as CLIMOND (Kriticos *et al.*, 2012), CHELSA (Karger *et al.*, 2017), CSIRO (Gordon *et al.*, 2010), WORLDCLIM (Fick and Hijmans, 2017), CR2MET (Boisier *et al.*, 2018), CAMELS-CL (Alvarez-Garreton *et al.*, 2018) and Pliscoff *et al. (*2014).

Finally, the need for climatic information spatially distributed in the Arica-Parinacota and Tarapacá region for environmental management or decision-making, highlights the importance of generating climate mapping, independent of the spatial variability and insufficient station coverage. The main objective was to determine different climatic characterization zones using topoclimatic analysis models. Also show the spatial variation of monthly and annual mapping of precipitation, average temperature, and solar radiation.

2. Materials and Methods

2.1. Study area

The study area (Fig. 1) is the regions of Arica-Parinacota and Tarapacá in the northern zone of Chile (17°30' to 21°38' S; 70º22' to 68°24' W), varying in altitude from 0 to 5200 meters of altitude,

with an arid to semi-arid climate influence on the coast by the Southeast Pacific Subtropical Anticyclone (SPSA), which generates high atmospheric stability, influenced by the Humboldt current that generates cold upwellings, causing a thermal inversion of up to 900 meters of altitude. In the pampas (large areas between valleys or ravines, from 300 to 1500 meters of altitude) there are arid conditions caused by the little penetration of clouds due to coastal thermal inversion, generating dry conditions and atmospheric transparency (Sarricolea and Romero, 2015). This cooling generates frequent clouds on the coast that advance inland only through the valleys ascending towards the foothills (up to 2000 meters of altitude). The highest mountains (over 3800 meters of altitude) represent a border that divides the eastern zone or Altiplano and the western zone from the foothills to the Pacific Ocean.

In the Altiplano area the SPSA loses its influence allowing the incursions of tropical air masses in the summer, that transports clouds and precipitation between November and March (Garreaud *et al.*, 2003) when they advance towards the west, the air masses losses their influence reducing up to 30% of relative humidity in foothills. The mean annual precipitation ranges from 5 mm to 600 mm in the eastern part. The precipitation variability in the Altiplano is high between seasons (Romero *et al.,* 2013) with alternation of wet and dry years strongly related to the Southern El Niño Southern Oscillation (ENSO) (Garreaud and Aceituno, 2001; Romero *et al.*, 2013). In the Altiplano (18°-27°S) there is a semi-arid climate determined by altitude at 3700 m., influenced by wet subtropical air masses in summer and cold air masses from the west with low relative humidity in winter (30%) (Aceituno, 1996; Garreaud, 2011). Average temperatures in summer are slightly above 10°C, while in winter they are below 6°C (Morales *et al.*, 2015). Solar radiation increases its value from the coast to the Altiplano. On the coast, due to the anticyclone influence, it has values between 16 to 18 MJ m^{-2} day^{-1}. In the pampas at 1500 meters of altitude there are values from 21 to 23 MJ m^{-2} day^{-1}. The values in the Altiplano exceed 23 MJ m^{-2} day^{-1}, however in summer cloudiness predominates with values close to 18 MJ m^{-2} day^{-1} as a daily average (Aceituno, 1996; Garreaud, 2011; Minvielle and Garreaud, 2011).

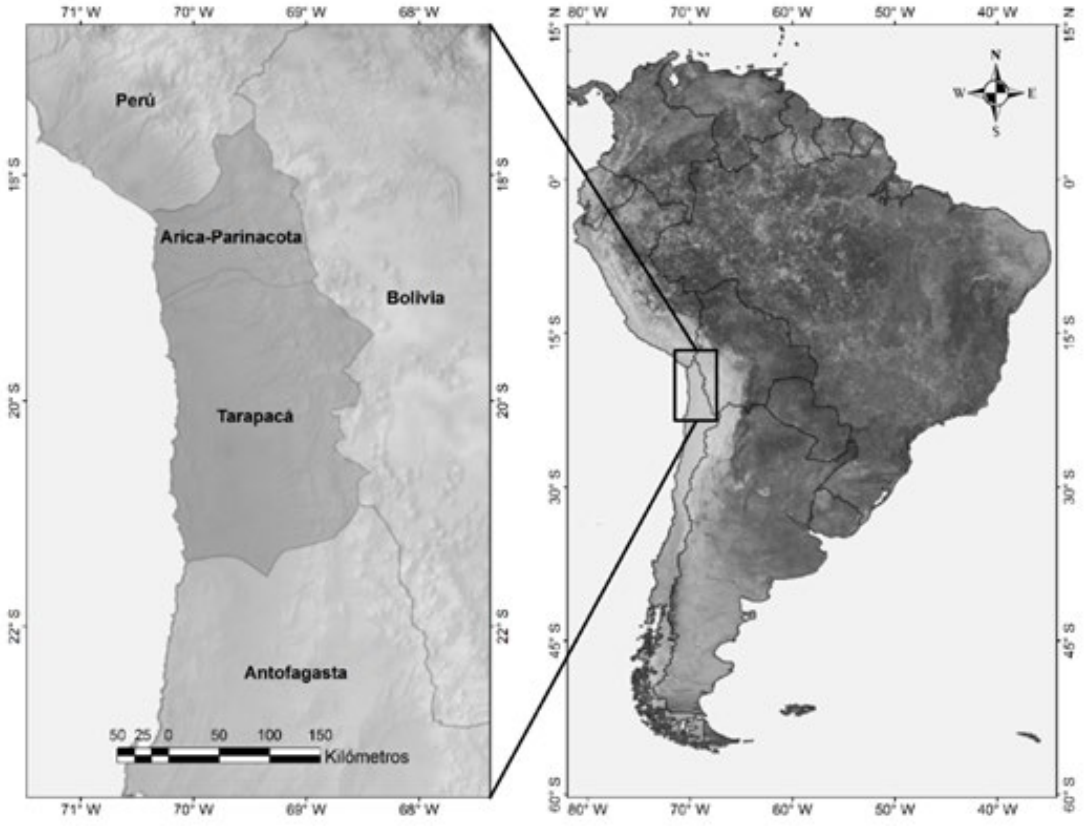

Figure 1. The study area that comprehends the Arica-Parinacota and Tarapacá regions.

2.2. Physiographic information

The climatic mapping needs a continuous database; thus, we only consider the meteorological stations with 10 or more years of continuous measurements from the following historical yearbooks sources: (Programa Desarollo Naciones Unidas (PNUD) and Gobierno de Chile, 1964; Luebert and Pliscoff, 2006; Matsuura and Willmott, 2009, 2012; Dirección General de Aguas, 2010; Dirección Meteorológica de Chile, 2018). The information source corresponds to data from government entities and scientific studies. Figure 2 show the spatial distribution of the meteorological stations used to obtain topoclimatic models for Temperature (28 stations), Precipitation (40 stations) and Solar Radiation (17 stations).

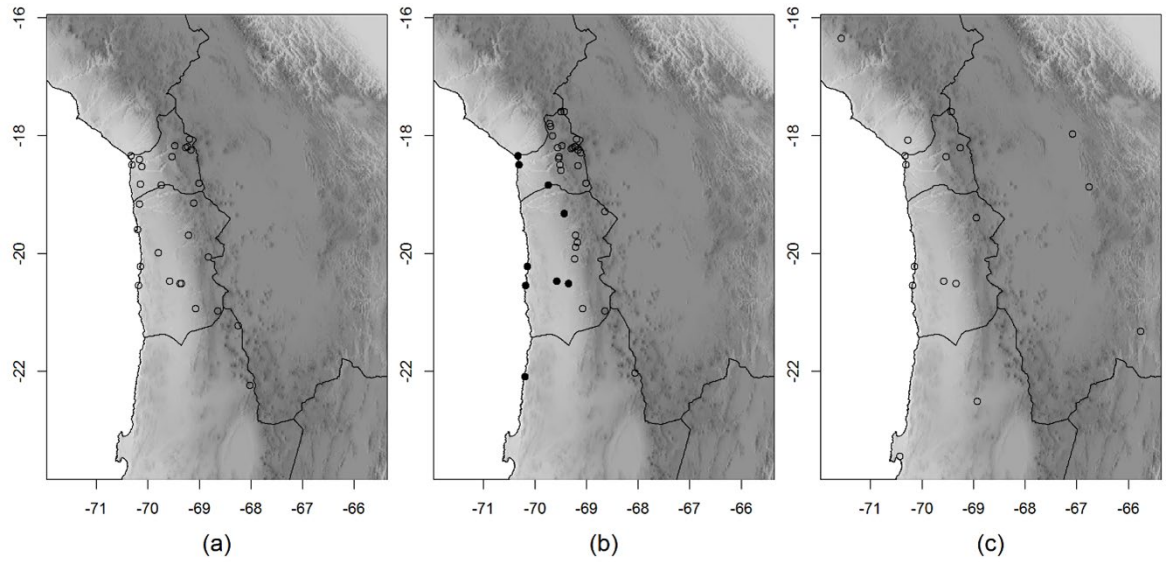

Figure 2. Data from the meteorological stations (a) Temperature, (b) precipitation (S1 black points with 9 stations, S2 white points with 31 stations) and (c) solar radiation. Source: (Santibañez, 1982; Dirección General de Aguas (DGA), 2010; Dirección Meteorológica de Chile (DMC), 2018).

The Spatial mapping used a digital terrain model (DTM) in a raster format, to obtain the following physiographic variables: latitude (LAT), longitude (LON), the distance to water bodies/salt flats (DW), and distance to the coast (DC). The DTM corresponds to The Shuttle Radar Topography Mission (SRTM), developed by the United States Geological Survey (Gesch *et al.*, 2014), with a spatial resolution of 90 m of the pixel size. All climatic and spatial information was projected to Datum WGS84 in geographic coordinates. The cartography was elaborated by the determination of topoclimatic equations using the IDRISI® program (Eastman, 2006) and the R statistical program (R Core Team, 2020).

2.3. Topoclimatic Modeling

The modeling of the different climatic variables was realized by applying the mathematical model described in the equation (1).

$$F(x_1, x_2, x_3, \ldots\ldots, x_n) = \sum_{j,k,n,m=0} a_j x_{k_1}^{n_1} x_{k_1}^{n_1} \ldots\ldots x_{k_n}^{n_m} \quad (1)$$

where F (x1, x2,...xn) represents a climatological variable in any period, x is a descriptive variable (LAT º, LON º, DC (km), DW (km), and ALT (meters); finally, aj are the coefficients to be determined

(Morales, 1997; Canessa, 2006; Morales *et al.*, 2006; Qiyao *et al.*, 2007; Diaz *et al.*, 2010; Cortez *et al.*, 2021). With the equations obtained, data matrices were calculated for each climatological variable in a binary matrix format on a monthly time scale.

To estimate the monthly mean temperature (*Tmonth*, °C) and annual mean temperature (*Tyear*, °C), the equation (2) was adjusted using independent variables LAT, LON, ALT, DC, and DW, reducing it to the following expression.

$$T = \sum_{i=0}^{n} b_i x_i \tag{2}$$

where T represents *Tmonth* or *Tyear*, x_i corresponds to the predictor variables (LAT, LON, ALT, DC, and DW) and b_i represents the coefficients of the multiple regression corresponding to each variable.

The fit of a general model of precipitation spatial distribution to the study area was a complex process, because of the different nature of precipitation, for this reason, the study area was divided into two sectors. Sector 1 (S1) represents the zone between the coast and the 2000 meters of altitude with 9 stations, while Sector 2 (S2) is the zone over 2000 meters that includes foothills, Altiplano, and high mountains with 31 stations. Between these two zones was the 10 millimeters isohyet, where the precipitation has an accelerated increase derived from convective precipitation in the Altiplano. (Sarricolea and Romero, 2015; Sarricolea *et al.*, 2017).

In each area, the spatial adjustment of the precipitation spatial models of the monthly mean (*Pmonth*, mm) was carried out following the methodology used by Canessa (2006). The *Pmonth* was estimated based on the mean annual precipitation (*Pyear*, mm), whose model was fitted spatially considering meteorological data and isohyets. To explain the spatial *Pyear* fitting the equation:

$$P_{year_{S1}} = \sum_{i=0}^{n} b_i x_i \tag{3}$$

$$P_{year_{S2}} = e^{(b_0 x_0 + b_1 x_1 + \cdots + b_n x_n)} \tag{4}$$

where x_1, x_2, and x_3 are the physiographical variables obtained from DTM models. b_0, b_1, b_2, and b_3, are the multiple regression coefficients. Then, the partition coefficients of annual precipitation (cr_j) were calculated, between the precipitation of each month (*Pmonth*) is divided by *Pyear*, according to the equation (5).

$$cr_j = \frac{P_{month_j}}{P_{year}} \tag{5}$$

The partition coefficients of *Pmonth* were fitted spatially according to the equation (5). Using the partition coefficients of monthly precipitation, it was possible to calculate the *Pyear* mapping. Additionally, the border between two zones (S1 and S2) of *Pyear* mapping was smoothed using a raster media filter (7x7).

A spatial variability of the Solar Radiation model was adjusted to estimate the mean annual solar radiation (*Ryear*) using the variables LAT, LON, ALT, and DC. The mean monthly solar radiation (*Rmonth*) was calculated according to the global partition coefficient in this zone for a month using the annual mean solar radiation data from meteorological stations and *Ryear* spatial fitting. The month partition coefficients were based on month precipitation data that were homogeneous with variation coefficients less than 15%.

2.4. Climate databases

The databases evaluated were: CLIMOND (Kriticos *et al.*, 2012), CHELSA (Karger *et al.*, 2017), CSIRO (Gordon *et al.*, 2010) WORLDCLIM (Hijmans *et al.*, 2005; Fick and Hijmans, 2017), CR2MET (Boisier *et al.*, 2018), CAMELS-CL (Alvarez-Garreton *et al.*, 2018) and Pliscoff *et al.* (2014). All databases had wide coverage of the study area, and of the limits, that allows to obtain values without of the border effect.

2.5. Statistical Analysis

The analysis of the results was carried out by comparing the predicted values (*Pi*) with the observed values (*Oi*) of the different climatic databases evaluated. For this analysis, the statistics systematic error (BIAS), mean absolute error value (MAE), mean square error (RMSE), Pearson determination coefficient (r^2), the agreement index (d) and the Akaike Information Criterion (AIC) were used (Table 1).

Table 1. Statistical criteria use to evaluate the performance of the spatial distribution model.

Index	Equation	Number
Systematic Error	$BIAS = \frac{1}{n}\sum_{i=1}^{n}(O_i - P_i)$	6
Root means square error	$RMSE = \sqrt{\frac{1}{n}\sum_{i=1}^{n}(O_i - P_i)^2}$	7
Agreement index	$d = 1 - \frac{\sum_{i=1}^{n}(O_i - P_i)^2}{\sum_{i=1}^{n}(\lvert P_i - \bar{O}\rvert - \lvert O_i - \bar{O}\rvert)^2}$	8
Mean absolute error value	$MAE = \sqrt{\frac{1}{n}\sum_{i=1}^{n}\lvert O_i - P_i\rvert}$	9
Pearson determination coefficient	$r^2 = \left[\frac{\sum_{i=1}^{n} O_i P_i - \frac{\sum_{i=1}^{n} O_i \cdot \sum_{i=1}^{n} P_i}{n}}{\sqrt{\sum_{i=1}^{n} {O_i}^2 - \frac{(\sum_{i=1}^{n} O_i)^2}{n}} \cdot \sqrt{\sum_{i=1}^{n} {P_i}^2 - \frac{(\sum_{i=1}^{n} P_i)^2}{n}}}\right]^2$	10
Akaike Information criterion	$AIC = 2 \cdot k - n \cdot Ln(L)\ or\ AIC = 2 \cdot k - n \cdot Ln\left(\frac{\sum_{i=1}^{n}(O_i - P_i)^2}{n}\right)$	11

O: Observed data, P: Predicted data, $\bar{O}$: Observed Data Average, n: sample size, k is the number of independent variables used and L is the log-likelihood estimate.

3. Results and discussion

3.1. Temperature

The models accounted for between 95 and 98% of the observed spatial variability in temperature. Table 2 shows the coefficients of the regression variables. We observed that the monthly coefficients for DC only show positive values, while DC2 and ALT2 had negative coefficients, while the other coefficients could be negative or positive depending on the month. It is important to mention the relation between the coefficients of DC and DC2 (b2 and b8, respectively) that results in change in the temperature behavior and coincides with a gradual decrease in *Tmonth* and *Tyear* when there is an increase in altitude towards the foothills between 2000 to 3500 m (Romero *et al.*, 2013). The standard error was between 0.9 and 1.4ºC, with lower values in the summer months. Figure 3 shows the relation

between the estimated and the observed values, with a determination coefficient of 0.978 with *Tyear* and *Tmonth*.

Table 2. The topoclimatical coefficients for the annual spatial distribution model of Temperature (Tyear), Precipitation (Pyear)* and Solar Radiation (Ryear)*.*

		Tyear	**Pyear S1**	**Pyear S2**	**Ryear**
b_0	Intercept	17.71	-704716.0	1499.530	-52315.90
b_1	ALT			-0.017	
b_2	DC	0.041	212.296	-1.740	
b_3	LAT		- 1561.170	82.920	
b_4	LON		- 19629.500	75.457	$4245 \cdot 10^5$
b_5	LAT^2		-0.570	1.016	$-202.883 \cdot 10^5$
b_6	LON^2		- 136.670	0.516	
b_7	ALT^2	$-8.591 \cdot 10^{-7}$			
b_8	DC^2	$-2.301 \cdot 10^{-4}$	-0.015	$1.594 \cdot 10^{-4}$	
b_9	LAT · LON		- 21.903		121.072
b_{10}	LAT · ALT		$-2.614 \cdot 10^{-4}$		$-1.987 \cdot 10^{-2}$
b_{11}	LAT · DC		2.948	-0.002	
b_{12}	LON · ALT		$7.522 \cdot 10^{-5}$	$-2.384 \cdot 10^{-4}$	
b_{13}	LON · DC		2.948	-0.024	-0.496
b_{14}	ALT · DC		$5.930 \cdot 10^{-5}$		
b_{15}	Ln |LAT|			825.424	$-3.866 \cdot 10^{-3}$
b_{16}	Ln |ALT|			5.189	

S1: defined the zone between the coast and under the 2000 m of altitude and S2 is the zone above this altitude, including the foothills, Altiplano, and high mountains.
* Statistically significant coefficient at 95% level.

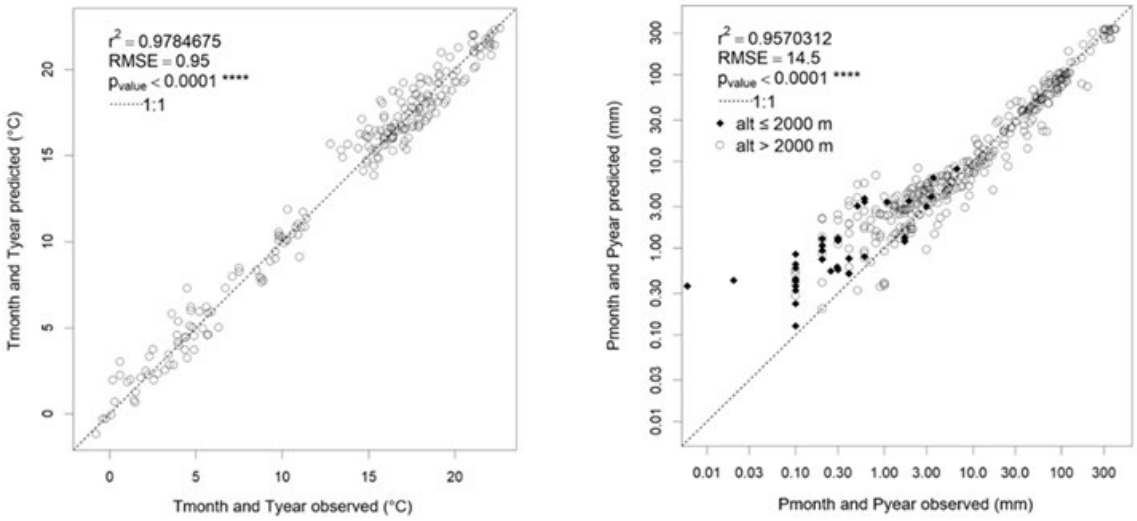

Figure 3. Observed values versus predicted of (a) Tmonth, Tyear, (b) Pmonth and Pyear.

Figure 4 shows the spatial pattern of *Tmonth* and *Tyear* in January and July. *Tyear* station values located at more than 3000 meters of altitude were below 10°C, while coastal stations such as Arica and Iquique *Tyear* were above 17°C. The influence of sea surface temperature and Pacific atmospheric pressure was most evident in coastal station values. In Caquena (4400 meters of altitude) the *Tyear* values were close to 0°C. The coast of the Atacama Desert was influenced by the Humboldt Current. Figure 4 also shows a spatial pattern in north-south strips, with a decreasing gradient towards the Andes Mountain (Romero *et al.*, 2013). This pattern highlights a warmer zone to the south of 20° latitude

(1100-1200 meters of altitude), which coincides with an oasis (Pica, Matilla, Esmeralda). Also, we can highlight a slight increase of *Tmonth* from the coast to the Coastal Range, which value was higher in July, according to the thermal inversion of the coast originating from the southeast Pacific anticyclone (Romero *et al.*, 2013; Sarricolea and Romero, 2015). There was a pattern that increases the temperature values to the south as in the intermediate depression, whose greatest difference was recorded in July, according to the thermal inversion of the coast originated for the southeast Pacific anticyclone (Romero *et al.*, 2013; Sarricolea and Romero, 2015).

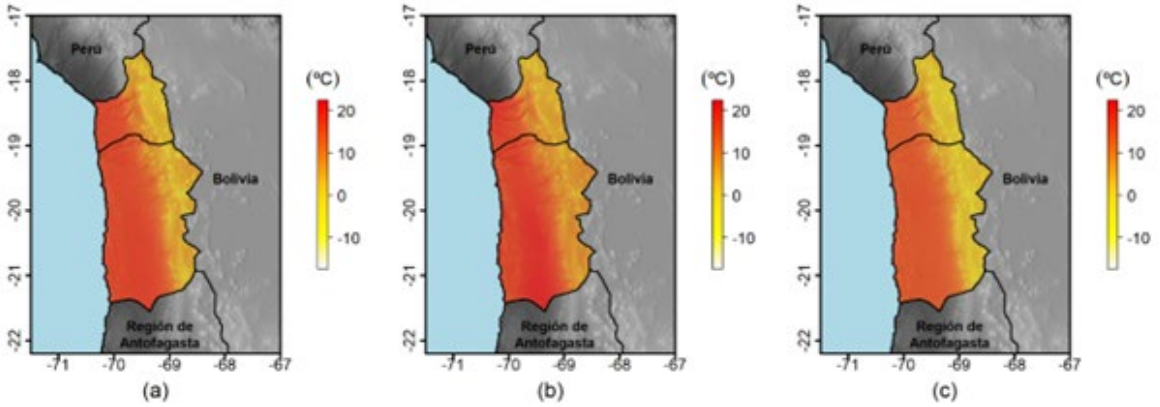

Figure 4. The spatial distribution of the Temperature (°C) estimated through the equation [6]: (a) Tyear, (b) Tmonth for January, and (c) Tmonth for July.

The maximum temperatures were observed in January in the pampas and the minimum in July. The spatial pattern has a decrease in the north-south stripes. Maximum temperatures were strongly related to the seasonal variability of surface solar radiation, whose maximum values coincided with the start of the rainy season (Romero *et al.*, 2013; Sarricolea and Romero, 2015). There were lower temperatures in July in the Altiplano due to a lower density of air and high solar radiation, which were associated with low relative humidity for almost the year. In summer this condition does not occur because there are convective storms that bring precipitation (Cereceda *et al.*, 2002).

Garreaud (2011) observed a closed thermal zone in the isotherm of 18ºC, located in the ravines, pampa of the south of 20º latitude. The area where it is below 5°C is less large than the area described by Aceituno (1996). This indicates that *Tyear* values were slightly lower and have a more geographical extent. Despite these differences attributable to the proposed method, the scale used in this study, we describe the trends of this area with great similarity in the coastal and foothills. It is important to mention that the validity of the adjusted model is only up to 4570 meters. The high mountains were not represented when in the process of the model fitting. In this sense, temperature values above 4570 meters of altitude may not adequately perceive the thermal behavior in this area (Garreaud, 2011).

The coastal temperature had a homogeneous pattern with a strong oceanic influence and moderating influence of the Humboldt current, also was influenced by El Niño (ENSO) and anomalies related to sea surface temperature (SST). The amounts of SST anomalies and the increments of the coastal temperature decrease from the tropical zone to the south (Montecinos *et al.*, 2003; Schulz *et al.*, 2012). The hottest and coldest years were often similar across seasons in this region. The warmest years coincide with the El Niño phenomenon (1983, 1992, 1997, 2006, and 2009), while the coldest years were following the La Niña phenomenon (1996, 1999, 2007, and 2010). At the coastal stations, with a more complete meteorological database, a decrease in the average temperature has been observed since 1999 (Romero *et al.*, 2013).

Table 3 analyses the performance of the models for *Tmonth* and *Tyear* against the observed values (the climate databases), it had a higher r2 and d, a lower MAE, RMSE, and AIC. The lowest value obtained from AIC is the criterion that allows us to say that it is the model that best fits all the previous ones for this area. However, the lowest bias or BIAS was obtained by WORLDCLIM2.

Table 3. Statistical performance of the estimation of the annual (Tyear) and monthly (Tmonth) spatial distribution of temperature.

Database	**Statistical Index**					
	BIAS	**MAE**	**RMSE**	**d**	**r^2**	**AIC**
CHELSA	-1.100	2.284	2.916	0.845	0.910	1590.9
CLIMOND	0.809	1.571	2.114	0.879	0.928	1395.2
CR2MET	0.719	1.595	2.034	0.885	0.939	1341.4
CSIRO	1.051	1.693	2.378	0.871	0.916	1459.1
Pliscoff *et al. (*2014)	0.131	1.684	2.147	0.872	0.914	1450.6
WORLDCLIM1	0.532	1.488	2.048	0.885	0.926	1395.1
WORLDCLIM2	0.317	1.344	1.835	0.896	0.939	1322.8
MODEL	0.382	1.077	1.354	0.918	0.968	1094.6

3.2. Precipitation

According to the methodology, two prediction models were generated to estimate the spatial distribution of *Pyear*, one for S1 defined under 2000 m of altitude and S2 above this altitude. According to Fig. 3, the two prediction models, and their coefficients were significant (r^2 equal to 0.910 for S1 and 0.996 for S2), although the number of stations present in sector S1 is lower than S2 (9 vs 31), there are also differences in precipitation values, with sector S1 being more stable than sector S2 The spatial pattern of the constructed database is represented in Figure 5.

Regarding the *Pyear* pattern, it could be said that there are values higher than 300 mm in the province of Parinacota (S2) whose precipitation is concentrated mostly between December to March. The values of *Pyear*, *Pmonth* in S1 for January and July decrease from north to south with a high variability of precipitation. This interannual variability coincides with ENSO cycles (Sarricolea and Romero, 2015). In S1 the conditions of aridity with precipitations less than 10 mm., were present in the sector of the Pampa, and on the coast, aridity is accentuated towards the region of Antofagasta, where the Atacama Desert is located.

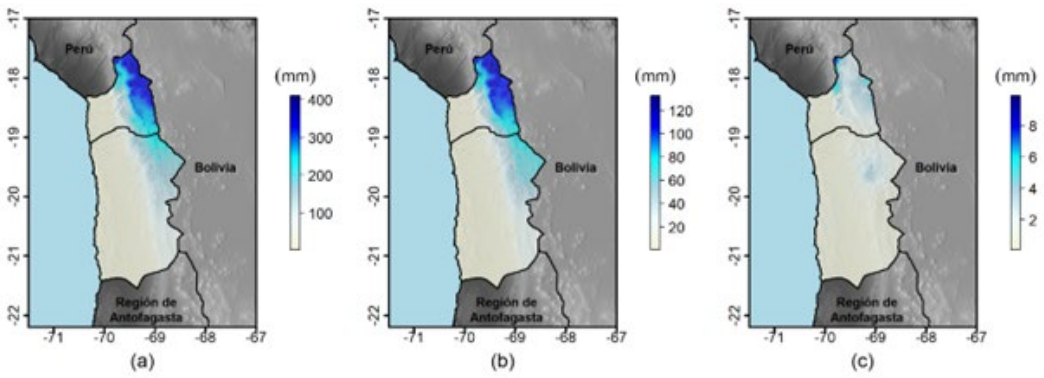

Figure 5. Spatial distribution of the Precipitation (mm) in the study area: (a) Pyear, (b) Pmonth of January, and (c) Pmonth of July.

Table 4 shows the statistical performance of the spatial distribution estimation for Precipitation. When we compare the *Pmonth* of every month and *Pyear* d the model built concerning the climate databases, it is the one with the highest r^2 and d, MAE, RMSE, and AIC lower. The lowest value obtained from AIC is the criterion that allows us to say that it is the model that best fits all the previous ones for this area. The second model that best represents precipitation is CHELSA.

Table 4. Statistical performance of the estimation of the annual (Pyear) and monthly (Pmonth) spatial distribution of Precipitation.

Database	**Statistical Index**					
	BIAS	**MAE**	**RMSE**	**d**	**r^2**	**AIC**
CHELSA	6.501	7.273	15.310	0.795	0.864	2957.0
CLIMOND	1.705	3.922	7.564	0.901	0.930	3086.2
CR2MET	0.956	4.118	8.636	0.897	0.907	3050.9
CSIRO	1.710	3.999	7.466	0.900	0.932	3083.5
Pliscoff *et al. (*2014)	2.089	4.407	9.513	0.885	0.894	3199.5
WORLDCLIM1	1.690	3.841	7.267	0.904	0.936	3049.1
WORLDCLIM2	1.400	3.908	7.294	0.902	0.935	3045.4
MODEL	1.190	3.366	7.038	0.914	0.946	2770.1

3.3. Solar Radiation

The *Rmonth* model and its coefficients were significant, where the coefficient of determination was 97.5 and the standard error was 0.7 MJ m^{-2} day^{-1} (Fig. 6)**.** Figure 7 show the *Rmonth* map obtained from the topoclimatic model. The independent variables and their coefficients are shown in Table 5. The LAT and LON were present in most of the calculated variables. The Figure 7 show a north-south pattern with values increasing towards to east up 19º parallel where this pattern is contracted towards the east. This behavior results in an east-west strip with values decreasing towards the north. The river courses have *Ryear.*

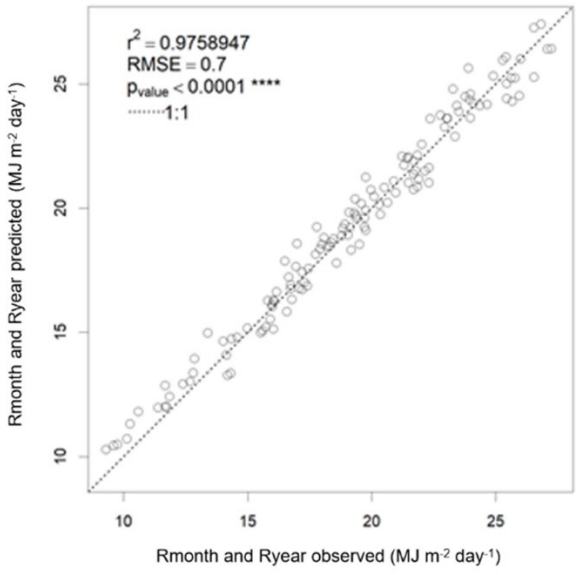

Figure 6. Observed values versus predicted for Rmonth and Ryear.

Table 5. Statistical performance of the estimation of the annual (Ryear) and monthly (Rmonth) spatial distribution of Solar Radiation.

Database	Statistical Index					
	BIAS	**MAE**	**RMSE**	**d**	**r^2**	**AIC**
CSIRO	3.514	3.663	4.129	0.520	0.752	878.93
WORLDCLIM2	0.807	1.615	2.259	0.755	0.756	838.02
MODEL	-0.148	0.587	0.700	0.916	0.976	269.55

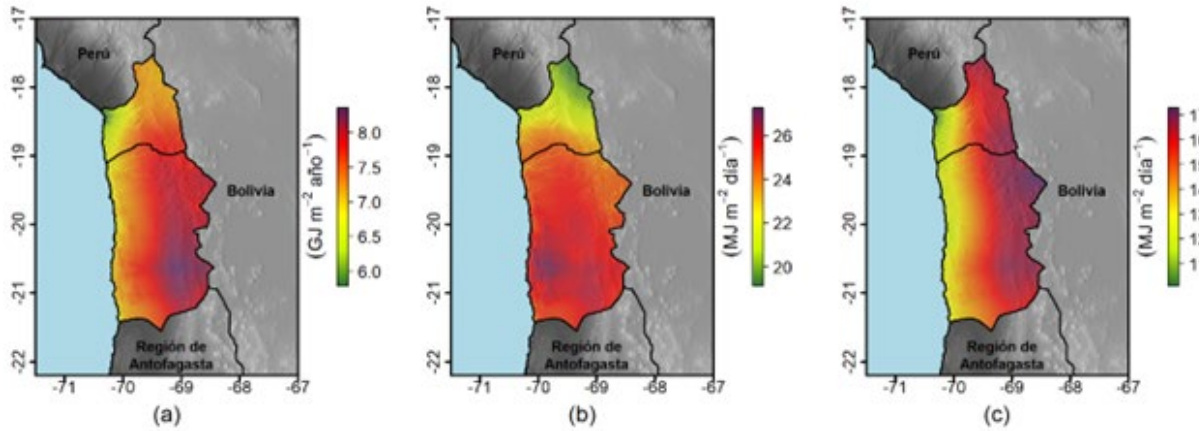

Figure 7. Spatial distribution of the Solar Radiation (MJ m-2 day-1) in the study area: (a) Ryear, (b) Rmonth of January, and (c) Rmonth of July.

Certain trends have been documented as the relationship between *Ryear* and cloudiness. The highest values of *Ryear* values were caused by the absence of cloudiness most of the year (Huber, 1977; Santibañez, 1982) and the *Ryear* decreased to the north from the south (Huber, 1977). By the other hand, *Ryear* mapping did not have significant changes regarding to relief shapes. The pattern of *Ryear* was smoother than *Pyear* and *Tyear* patterns.

For the *Ryear* pattern, the topographic variables LAT, LON, and DC were most significative than ALT. This excludes relief factors such as slope or solar exposure that modify the spatial pattern of solar radiation (Sarricolea and Romero, 2015). The cloudiness increases during the rainfall season (December to March), while the maximum solar radiation values were reached during the spring-summer season, where the Visviri station registered a maximum of 1000 W m^{-2} (Aceituno, 1996).

Huber (1977) and Santibañez (1982) show similar behavior in isotherms (*Tyear*) and isohyets (*Pyear*). However, they show lower values at the coast, which is a zone with high cloudiness frequency, than in our study. The *Ryear* values were remarkably similar in the southern regions over 1200 meters of altitude.

When we compare the estimation of *Rmonth* and *Ryear* with the climate databases, it is the one with the highest r^2 and d, and an MAE, RMSE and AIC lower. The lowest value obtained from AIC is the criterion in which it allows us to say that it is the model that best fits of all the previous ones for this area. There were no major differences between the other two models evaluated. The scarcity of solar radiation information in the study area implies restriction to determinate bioclimatic indicators, such as the Evapotranspiration or the Aridity Index.

4. Conclusion

Topoclimatic models allow describing the spatial variability of temperature, precipitation, and solar radiation in the regions of Arica-Parinacota and Tarapacá, depending on the relief and spatial coordinates (latitude and longitude). Altitude and distance to the coast were significant for estimating the spatial distribution of temperature, while for precipitation the most important variables were latitude and distance to the coast; finally, latitude, longitude, and distance to the coast were relevant to predict solar radiation. Both temperature and precipitation show clear variations across relief and geomorphological stripes, however, solar radiation has a pattern highly linked to spatial location. The main role of the Andes Mountain range in the delimitation of the zone of high annual rainfall stands out. The usefulness of the topoclimatic models based on the climatic variables allows a good interpolation and estimation of the spatial variability at monthly and/or annual means. The topoclimatic models developed had greater significance than other climate databases. This work facilitates its use in local environmental or agronomic studies.

Acknowledgment

Special thanks to FIC program PIT-2008-0189 of University of Chile, FIC program 30170072-0 of Agriculture Research Institute (INIA) and 1795 agreement of Universidad de Chile.

References

Aceituno, P., 1996. Elementos del clima en el Altiplano Sudamericano. *Rev. Geofísica 44*, 37–55.

Alvarez-Garreton, C., Mendoza, P.A., Boisier, J.P., Addor, N., Galleguillos, M., Zambrano-Bigiarini, M., Lara, A., Puelma, C., Cortes, G., Garreaud, R., McPhee, J., Ayala A., 2018. The CAMELS-CL dataset: catchment attributes and meteorology for large sample studies–Chile dataset. *Hydrology and Earth System Sciences 22*(11), 5817–5846. http://doi.org/10.5194/hess-22-5817-2018

Boisier, J.P., Alvarez-Garretón, C., Cepeda, J., Osses, A., Vásquez, N., Rondanelli, R., 2018. CR2MET: A high-resolution precipitation and temperature dataset for hydroclimatic research in Chile. In *EGU General Assembly Conference Abstracts*, p. 19739.

Burkhard, B., Maes, J., 2017. *Mapping Ecosystem Services*. In: B Burkhard, J. Maes, Eds.) *Advanced Books* (Vol. 1). Pensoft Publishers.

Canessa, F., 2006. *Evaluación de los recursos climáticos de la IV Región de Coquimbo, mediante la utilización de Topoclimatología e imágenes NOAA-AVHRR*. Universidad de Chile, Facultad de Cs. Agronómicas, Chile.

Cereceda, P., Osses, P., Larrain, H., Farías, M., Lagos, M., Pinto, R., Schemenauer, R.S., 2002. Advective, orographic and radiation fog in the Tarapacá region, Chile. *Atmospheric Research 64*(1–4), 261–271. http://doi.org/10.1016/S0169-8095(02)00097-2

Cortez, D., Herrera, S., Araya-Osses, D., Caroca, C., Padilla, R., Uribe, J., Paneque, M., 2021. Topoclimatic zoning of continental Chile. *Journal of Maps 17*(2), 114–124. https://doi.org/10.1080/17445647.2021.1886188

Daly, C., Halbleib, M., Smith, J.I., Gibson, W.P., Doggett, M.K., Taylor, G.H., Curtis, J., Pasteris, P.P., 2008. Physiographically sensitive mapping of climatological temperature and precipitation across the conterminous United States. *International Journal of Climatology* 28(15), 2031–2064. http://doi.org/10.1002/joc.1688

Diaz, D., Morales, L., Castellaro, G., Neira, F., 2010. Topoclimatic Modeling of Thermopluviometric Variables for the Bío Bío and La Araucanía Regions, Chile. *Chilean Journal of Agricultural Research 70*(4), 604–615. [En línea]. https://oes.chileanjar.cl/files/V70_I4_2010_ENG_DiegoDiazM.pdf (Last access: 29/11/2022).

Dirección General de Aguas (DGA), 2010. Plan de Acción Estratégico para el Desarrollo Hídrico de la región de Arica y Parinacota. *Ministerio de Obras Púbicas, Gobierno de Chile*, 90.

Dirección Meteorológica de Chile (DMC), 2018. *Anuarios Decadales.*

Eastman, J.R., 2006. *IDRISI Andes: Guide to GIS and Image Processing*. Worcester: Clark Labs, Clark University.

Fick, S.E., Hijmans, R.J., 2017. WorldClim 2: new 1-km spatial resolution climate surfaces for global land areas. *International Journal of Climatology 37*(12), 4302–4315. https://doi.org/10.1002/joc.5086

Florinsky, I.V., 1998. Combined analysis of digital terrain models and remotely sensed data in landscape investigations. *Progress in Physical Geography: Earth and Environment 22*(1), 33–60. http://doi.org/10.1177/030913339802200102

Fredericksen, N., 2010. *Estimación de la capacidad de carga de los tipos vegetacionales con aptitud pastoral destinados al manejo de Vicuña (Vicugna vicugna Mol.), en el Altiplano de la Provincia de Parinacota, Región de Arica y Parinacota.* Universidad de Chile. Available at: https://repositorio.uchile.cl/handle/2250/112244 (Last access: 29/11/2022).

Garreaud, R., 2011. The Climate of Northern Chile: mean state, variability and trends. "Astronomical Site Testing Data Conference in Chile." *Revista Mexicana de Astronomía y Astrofísica (SC)* 41, 5–11.

Garreaud, R., Aceituno, P., 2001. Interannual Rainfall Variability over the South American Altiplano. *Journal of Climate* 14(12), 2779–2789. http://doi.org/10.1175/1520-0442(2001)014<2779:IRVOTS>2.0.CO;2

Garreaud, R., Vuille, M., Clement, A.C., 2003. The climate of the Altiplano: Observed current conditions and mechanisms of past changes. *Palaeogeography, Palaeoclimatology, Palaeoecology* 194, 5–22). http://doi.org/10.1016/S0031-0182(03)00269-4

Gesch, D. B., Oimoen, M.J., Evans, G.A., 2014. *Accuracy assessment of the US Geological Survey National Elevation Dataset, and comparison with other large-area elevation datasets: SRTM and ASTER* (Vol. 1008). US Department of the Interior, US Geological Survey. https://doi.org/10.3133/ofr20141008

Gordon, H.B., O'Farrell, S., Collier, M., Dix, M., Rotstayn, L., Kowalczyk, E., Hirst, T., Watterson, I., 2010. *The CSIRO Mk3. 5 climate model* (Vol. 74). CSIRO and Bureau of Meteorology. Available at: http://www.bom.gov.au/research/publications/cawcrreports/CTR_021.pdf (Last access: 29/11/2022).

Grunwald, S., 2009. Multi-criteria characterization of recent digital soil mapping and modeling approaches. *Geoderma* 152(3), 195–207. https://doi.org/10.1016/j.geoderma.2009.06.003

Grunwald, S., Thompson, J.A., Boettinger, J.L., 2011. Digital Soil Mapping and Modeling at Continental Scales: Finding Solutions for Global Issues. *Soil Science Society of America Journal* 75(4), 1201–1213. http://doi.org/https://doi.org/10.2136/sssaj2011.0025

Harris, I., Jones, P., Osborn, T., Lister, D., 2014. Updated high-resolution grids of monthly *climatic observations–the CRU TS3. 10 Dataset. International Journal of Climatology* 34(3), 623–642. https://doi.org/10.1002/joc.3711

Hijmans, R., Cameron, S., Parra, J., Jones, P., Jarvis, A., 2005. Very high-resolution interpolated climate surfaces for global land areas. *International Journal of Climatology* 25(15), 1965–1978. https://doi.org/10.1002/joc.1276

Huber, A., 1977. Aporte a la climatología y climaecología de Chile. I: Radiación Potencial. II: Radiación Efectiva. *Medio Ambiente* 3(1), 3–14.

Hunter, R., Meentemeyer, R., 2005. Climatologically aided mapping of daily precipitation and temperature. *Journal of Applied Meteorology* 44(10), 1501–1510. https://doi.org/10.1175/JAM2295.1

Kaminski, A., Radosz, J., 2005. Topoclimatic mapping on 1:50000 scale, the map sheet of Bytom. Available at: http://meteo.geo.uni.lodz.pl/icuc5/text/P_8_1.pdf (Last access: 29/11/2022).

Karger, D.N., Conrad, O., Böhner, J., Kawohl, T., Kreft, H., Soria-Auza, R.W., Zimmermann, N.E., Linder, H.P., Kessler, M., 2017. Climatologies at high resolution for the earth's land surface areas. *Scientific Data* 4(1), 1–20. https://doi.org/10.5061/dryad.kd1d4

Kaye, N.R., Hartley, A., Hemming, D., 2012. Mapping the climate: guidance on appropriate techniques to map climate variables and their uncertainty. *Geoscientific Model Development* 5(1), 245–256. http://doi.org/10.5194/gmd-5-245-2012.

Kriticos, D.J., Webber, B.L., Leriche, A., Ota, N., Macadam, I., Bathols, J., Scott, J.K., 2012. CliMond: global high-resolution historical and future scenario climate surfaces for bioclimatic modelling. *Methods in Ecology and Evolution* 3(1), 53–64. https://doi.org/10.1111/j.2041-210X.2011.00134.x

Luebert, F., Pliscoff, P., 2006. *Sinopsis bioclimática y vegetacional de Chile.* Editorial Universitaria.

Luebert, F., Pliscoff, P., 2018. *Sinopsis bioclimática y vegetacional de Chile* (Second). Santiago: Editorial Universitaria.

Matsuura, K., Willmott, C.J., 2009. Terrestrial air temperature: 1900–2008 gridded monthly time series. *Center for Climatic Research, Dep. Of Geography, University of Delaware, Newark.* Available at: http://climate.geog.udel.edu/~climate/html_pages/Global2_Ts_2009/README.global_t_ts_2009.html (Last access: 29/11/2022).

Matsuura, K., Willmott, C.J., 2012. Terrestrial precipitation: 1900-2010 gridded monthly time series. Available at: http://climate.geog.udel.edu/~climate/html_pages/Global2011/Precip_revised_3.02/README.GlobalTsP2011.html (Last access: 29/11/2022).

Minvielle, M., Garreaud, R., 2011. Projecting rainfall changes over the South American Altiplano. *Journal of Climate* 24(17), 4577–4583. http://doi.org/10.1175/JCLI-D-11-00051.1

Montecinos, A., Purca, S., Pizarro, O., 2003. Interannual-to-interdecadal sea surface temperature variability along the western coast of South America. *Geophysical Research Letters* 30(11). http://doi.org/10.1029/2003GL017345

Morales, L., 1997. *Evaluación y zonificación de riesgos de heladas mediante modelación topoclimática.* Universidad de Concepción.

Morales, L., Canessa M.F., Mattar, C., Orrego, R., Matus, F., 2006. Caracterización y Zonificación Edáfica y Climática de la Región de Coquimbo, Chile. *Revista de La Ciencia Del Suelo y Nutrición Vegetal*.

Morales, L., Acevedo, E., Castellaro, G., Roman, L., Morales-Inostroza, J., Alonso, M., 2015. A simple method for estimating suitable territory for bioenergy species in Chile. *Ciencia e Investigación Agraria* 42(2), 227–242. http://doi.org/10.4067/S0718-16202015000200009

Pliscoff, P., Luebert, F., Hilger, H., Guisan, A., 2014. Effects of alternative sets of climatic predictors on species distribution models and associated estimates of extinction risk: A test with plants in an arid environment. *Ecological Modelling* 288, 166–177. https://doi.org/10.1016/j.ecolmodel.2014.06.003

Programa de Desarrollo de Naciones Unidas (PNUD) and Gobierno de Chile, 1964. *Gobierno de Chile. Proyecto Hidrometeorológico. Climatología en Chile. Fascículo I. Valores normales de 36 estaciones seleccionadas. Período 1916-1945. s.e. Santiago de Chile. s.p.*

Qiyao, L., Jingming, Y., Baopu, F., 2007. A method of agrotopoclimatic division and its practice in China. *International Journal of Climatology* 11, 85–96. http://doi.org/10.1002/joc.3370110107

R Core Team, 2020. R: *A language and environment for statistical computing.*

Romero, H., Smith, P., Mendonça, M., Méndez, M., 2013. Macro y mesoclimas del altiplano andino y desierto de Atacama: desafíos y estrategias de adaptación social ante su variabilidad. *Revista de Geografía Norte Grande* 55, 19–41. http://doi.org/10.4067/S0718-34022013000200003

Santibañez, F., 1982. Zonificación de los recursos climáticos de la I Región. Capítulo I. Análisis de los ecosistemas de la Primera Región de Chile. In: F. Santibañez, M. Etienne and S. Lailhacar (Edrs.). *Delimitación y caracterización de los ecosistemas de la I región de Chile.* Santiago, Chile: Sociedad Agrícola CORFO-SACOR.

Sarricolea, P., Romero, H., 2015. Variabilidad y cambios climáticos observados y esperados en el Altiplano del norte de Chile. *Revista de geografía Norte Grande* 62, 169–183. http://doi.org/10.4067/S0718-34022015000300010

Sarricolea, P., Meseguer Ruiz, O., Romero-Aravena, H., 2017. Tendencias de la Precipitación en el Norte Grande de Chile y su relación con las Proyecciones de Cabio Climático. *Diálogo Andino* 54, 41–50. http://doi.org/http://dx.doi.org/10.4067/S0719-26812017000300041

Schulz, N., Boisier, J.P., Aceituno, P., 2012. Climate change along the arid coast of northern Chile. *International Journal of Climatology* 32(12), 1803–1814. http://doi.org/10.1002/joc.2395

Skirvin, S.M., Marsh, S.E., McClaran, M.P., Meko, D.M., 2003. Climate spatial variability and data resolution in a semi-arid watershed, south-eastern Arizona. *Journal of Arid Environments* 54(4), 667–686. http://doi.org/10.1006/jare.2002.1086